

See discussions, stats, and author profiles for this publication at: <https://www.researchgate.net/publication/231651416>

Ion-Exchanged Binuclear Clusters As Active Sites of Selective Oxidation over Zeolites

ARTICLE *in* THE JOURNAL OF PHYSICAL CHEMISTRY C · MAY 2009

Impact Factor: 4.77 · DOI: 10.1021/jp808449w

CITATIONS

13

READS

19

4 AUTHORS:



Georgy Zhidomirov
Russian Academy of Sciences
402 PUBLICATIONS 2,651 CITATIONS

[SEE PROFILE](#)



Alexander Larin
Lomonosov Moscow State University
68 PUBLICATIONS 369 CITATIONS

[SEE PROFILE](#)



Dmitrii Trubnikov
Lomonosov Moscow State University
60 PUBLICATIONS 134 CITATIONS

[SEE PROFILE](#)



Daniel P Vercauteren
University of Namur
187 PUBLICATIONS 1,465 CITATIONS

[SEE PROFILE](#)

Ion-Exchanged Binuclear Clusters As Active Sites of Selective Oxidation over Zeolites

G. M. Zhidomirov,^{†‡} A. V. Larin,^{*,†} D. N. Trubnikov,[†] and D. P. Vercauteren[§]

*Department of Chemistry, Moscow State University, Moscow, GSP-2, 119992, Russia,
Boreskov Institute of Catalysis, SO RAN, Novosibirsk, 630090, Russia, and University of Namur (FUNDP),
Rue de Bruxelles 61, B-5000 Namur, Belgium*

Received: September 23, 2008; Revised Manuscript Received: February 05, 2009

A new catalytic oxidation cycle over binuclear Zn- and Ca-cation clusters in zeolites is proposed. Intermediate active clusters appear due to trapping of dioxygen. CO oxidation is considered as a model reaction over a cluster located in an 8-membered (8R) ring. Geometries of active clusters involved in the catalytic cycle vary depending on the nature and size of the cation. Reagents, transition states, and products have been optimized at the isolated cluster level considering DFT functionals (B3LYP, B3P86, and B3PW91) with the 6-31G* or 6-311++G** basis sets. Moderate activation energies of 23.0 and 35.7 kcal/mol at the B3LYP/6-31G* level are obtained for CO oxidation over Zn- and Ca-clusters, respectively.

Introduction

Oxidation by O₂ in zeolite forms with alkaline and alkaline earth cations has long been a topic of discussion with respect to various organic molecules.^{1–5} For example, oxidation of small alkenes,^{1–3} toluene,^{4,6} *p*-xylene,⁶ cyclohexane,^{5,7} and propane,⁸ and of CO within frameworks involving complex mechanisms with noble metal clusters⁹ has already been studied in details. As well, the case of CO oxidation in CaY seems also relevant even if O₂ is not directly used under experimental conditions.¹⁰ Oxidation over alkaline and alkaline earth cationic forms was considered as a different class compared to other oxidation reactions with O₂ participation.⁸ The mechanism is interpreted as a stabilization of an “organic molecule–O₂” ion pair with an essential charge transfer.^{1–5} The primary role of the electric field for such stabilization was hence emphasized for both alkaline and alkaline earth cations. The complex dependence of the reaction yield on the electric field cannot however ascertain a unique oxidation mechanism. Moreover, it is difficult to apply the idea of ion pair transition state with large charge transfer to the CO–O₂ case.

The appearance of the [M–O–M]²⁺ species with extra-lattice oxygen (ELO) is very probable upon increasing the Si/Al ratio of the zeolite framework as shown by both numerous experimental and theoretical studies. Experimental evidence was first found by Boudart and co-workers, who observed redox pairs of iron ions in FeY.¹¹ The bridging position of oxygen was confirmed by Mössbauer¹² and IR¹³ spectroscopy. The catalytic activity of such a system is associated with both the binuclear structure and peculiar chemical properties of ELO, which vary with the framework type. Much attention was paid to the redox properties of the binuclear structures¹⁴ that were assumed to be responsible for the kinetics of catalytic reactions, for example, the concentration oscillations of N₂O decompositions.^{15,16} The majority of theoretical studies relative to oxo-binuclear structures in zeolites were devoted to the structural and chemical properties of oxygen-bridged [Cu–O–Cu]²⁺ ion pairs, with regard to the problem of catalytic processes for selective NO_x reductions.^{17–20}

Oxo-bridged binuclear [Zn–O–Zn]²⁺ structures were discussed considering the problem of dehydrogenations of light alkanes.²¹ Finally, let us mention methanol to olefins (MTO) decomposition over [Fe–O–Fe]²⁺ studied in refs 22 and 23.

In this paper, another possible oxidation mechanism is suggested and discussed with respect to CO oxidation for Zn- and Ca-cation exchanged zeolites. Assuming the appearance of two closely located Si/Al replacements and two respective Me cations, we have found a series of new Me₂O_X (X = 1–3) oxide clusters which could serve as oxidation centers in zeolites.

First we describe the computational strategy which is modified versus the usual cluster approach while increasing the cluster size by adding and optimizing an extra layer of nearest O atoms. In the first part of the Results, we will discuss the optimized geometries and heats of formation. The main attention is paid to the comparison of the oxidation of CO over the Zn- and Ca-clusters in the Me₂O₂ form considering small and large clusters and various DFT functionals. In the last part of the Results, CO oxidation is studied over Ca₂O₃ at both the B3LYP and MP2 levels to evaluate the accuracy of the B3LYP computations.

Computational Details

First, we fully optimized the geometry of a supercell with two primitive cells of Zn-form of mordenite (MOR) using the GULP code²⁴ and Catlow force field (FF)^{25,26} with Al in position T4²⁷ on the opposite sides of the large channel in ZnMOR. One of the 8R rings which opens the side pockets in ZnMOR was isolated from the 3D structure and the second Si atom was replaced by Al at T4. Keeping the Zn cation near the 8R ring and filling the ruptured T–O bonds of all T atoms (T = Si and Al) by capping hydrogen atoms, one reached a neutral fragment ZnAl₂Si₆O₈H₁₆. The initial T–H bond lengths were fixed at 1.4 Å, close to the optimal value as estimated at the B3LYP/6-31G* level. The T–H lengths were further optimized using Gaussian 03²⁸ at fixed O–T–H and T’–O–T–H angles and fixed positions of the other atoms. Then, H atoms only were fixed and the coordinates of the other atoms were varied also at the B3LYP/6-31G* level, as most results obtained here.

An important step was then to check the influence of spatial restraints on the resulting energy and geometry for a larger fragment, obtained by addition of a layer of 16 oxygen atoms

* Corresponding author. E-mail: nasgo@yandex.ru.

[†] Moscow State University.

[‡] Boreskov Institute of Catalysis.

[§] University of Namur.

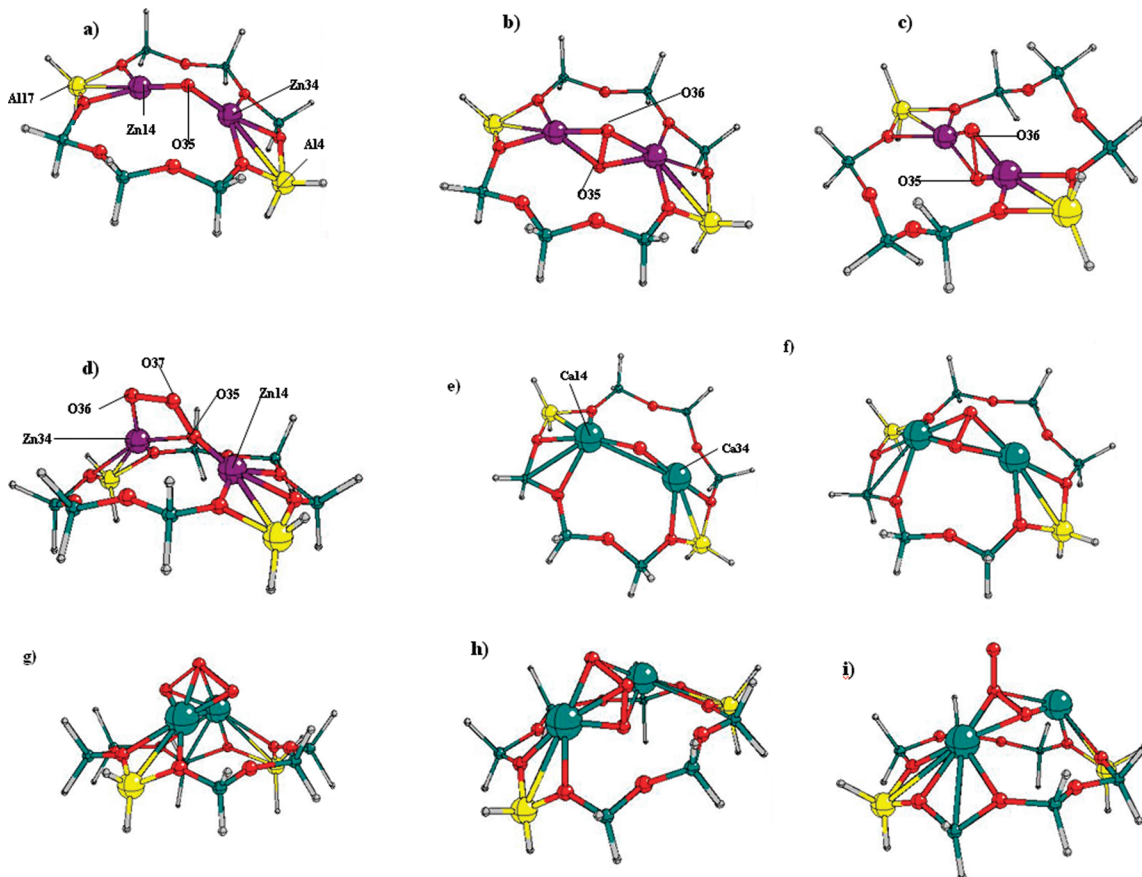


Figure 1. Structures of the small $\text{Me}_2\text{O}_X(8\text{R})$ clusters, $\text{Me} = \text{Zn}$ (a–d), $\text{Me} = \text{Ca}$ (e–i) for $X = 1$ (a, e), $X = 2$ (b, c, f), $X = 3$ (d, g, h, i) for restrained optimizations, i.e., with fixed H atoms as described in the text (a–b, d–i) or full optimizations (c). Rotated (h) and inverted (i) conformers of $\text{Ca}_2\text{O}_3(8\text{R})$ are also shown. Atomic labels of Figure 1 are used in Tables 1–3. The color code is: Zn in purple, Ca in green (larger spheres), O in red, Si in green (smaller spheres), Al in yellow, H in gray.

to the 8R ring T atoms instead of H. To add the O atoms, the optimized small cluster was embedded in the initial crystallographic position. It was achieved via a series of rotations of the small cluster as a whole, i.e., with fixed relative optimized coordinates in order to reach minimal distances between the O atoms in crystallographic positions and the optimized H atoms. The already optimized H atoms were replaced by the nearest O atoms in crystallographic positions while additional H atoms were added to the new O atoms in the direction of the nearest T atoms. Then the optimization procedure of the H coordinates was repeated as for the smaller cluster.

To determine the reaction coordinate for CO oxidation, we applied the QST3 algorithm as supplied with Gaussian 03²⁸ considering the optimized geometries of the reagents and products.

Results

Relative Stabilities and Geometries of the $\text{Me}_2\text{O}_X(8\text{R})$ Clusters. The bridge $[\text{Me}–\text{O}–\text{Me}]^{2+}$ geometry has already been discussed in the literature for $\text{Me} = \text{Zn}$,^{21,29} Cu,^{15,17–20} and Fe.^{16,22,23} Herein, different stationary geometries of Me_2O_X oxide clusters ($X = 1–3$) in cationic positions of the 8R ring were first optimized for $\text{Me} = \text{Zn}$ and Ca. The Zn_2O (Figure 1a) and Ca_2O (Figure 1e) models are quite similar while large differences are observed between Zn_2O_2 (Figure 1b) and Ca_2O_2 (Figure 1f) or between Zn_2O_3 (Figure 1d) and Ca_2O_3 (Figure 1g). These different geometries are mainly conserved at different stages of the CO oxidation presented below in detail (Figure 2). The Zn–O distances are shorter in the $\text{Zn}_2\text{O}(8\text{R})$ models (Table 1)

compared to those in $\text{Zn}_2\text{O}_2(8\text{R})$ (Table 2). For $\text{Ca}_2\text{O}(8\text{R})$, two pseudopotential basis sets for Ca were also tested denoting the appropriate quality of the LANL2DZ basis (Table 3), which however leads to higher atomic charges than the values obtained with 6-31G*.

If the existence of $[\text{Zn}–\text{O}–\text{Zn}]^{2+}$ is accepted conventionally in literature,^{21,29} it is not the case of $[\text{Ca}–\text{O}–\text{Ca}]^{2+}$. We therefore evaluated the respective exothermic effects of the $\text{Me}_2\text{O}(8\text{R})$ formation according to the reaction



It gave -52.3 and -85.3 kcal/mol at the B3LYP/6-31G* level for $\text{Me} = \text{Ca}$ and Zn , respectively, that can be considered as the thermodynamic confirmation of the $\text{Me}_2\text{O}(8\text{R})$ formation.

For the Zn cations, the optimized structures of Zn_2O_2 (Figure 1b) and Zn_2O_3 (Figure 1d) clusters are oriented in a plane that is nearly perpendicular to the 8R ring and that passes through both Zn cations. The possible parallel orientation of the O–O part versus the 8R ring was checked but it is not stable for the Zn complex. The rhomb Zn_2O_2 geometry is similar to the square type clusters that were optimized for Al_2O_2 ³⁰ and Ga_2O_2 .^{31,32} Due to spatial limits imposed by the larger ionic radii of Ca^{2+} (1.00 Å)³³ versus Zn^{2+} (0.74 Å), the rhomb Ca_2O_2 cluster is parallel to the 8R ring (Figure 1f) so that both O atoms of the peroxide O–O moiety are more accessible for adsorbate molecules as compared to the one of Zn_2O_2 (Figure 1b). The presence of the peroxide O–O part which can serve as an oxidizing reagent is the principal feature of the Zn_2O_2 and Ca_2O_2 clusters obtained herein versus Al_2O_2 ,³⁰ Ga_2O_2 ,^{31,32} and Zr_2O_3 .³⁴

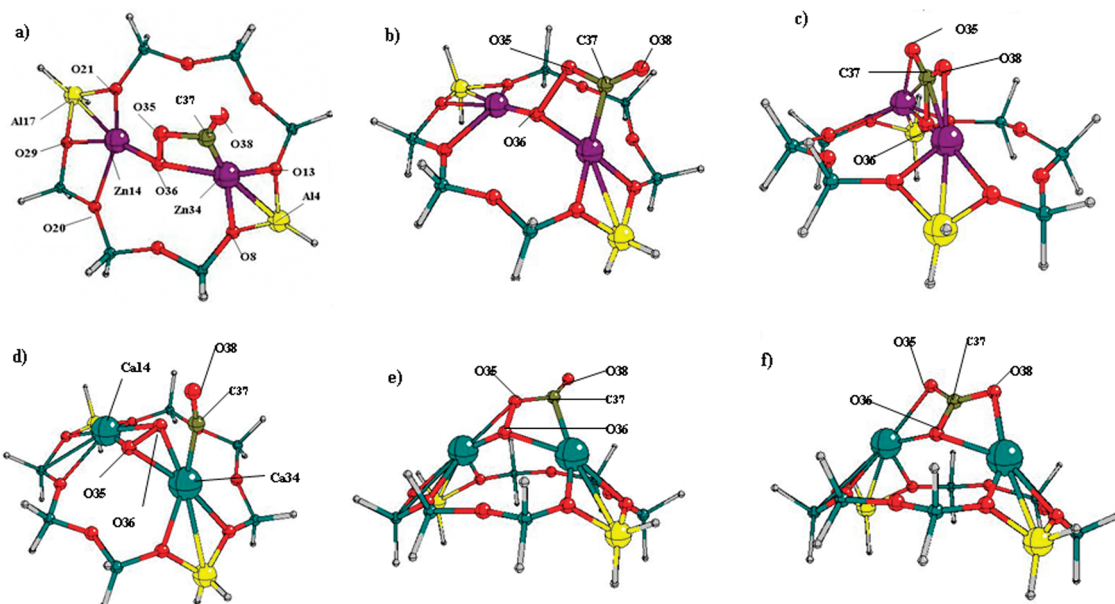


Figure 2. Structures of the reagent (a, d), transition state (b, e), and product clusters (c, f) for CO oxidation over the small optimized $\text{Me}_2\text{O}_2(8R)$ clusters, $\text{Me} = \text{Zn}$ (a–c), $\text{Me} = \text{Ca}$ (d–f). Atomic labels of Figure 2 are used in Tables 2 and 3. The color code corresponds to the one of Figure 1; C is in brown.

TABLE 1: Several Geometrical Parameters of the Me₂O(8R) Models (Distances in Å, Angles in Degrees) Calculated at the B3LYP Level with 6-31G^{*a}

parameter	Ca	Zn
Me34—O35	2.118	1.766
Me34...Al4	3.202	2.834
Me14—O35	2.115	1.783
Me14...Al17	3.247	2.945
Me14...Me34	3.746	3.247
Me14—O35—Me34	124.48	132.47

^a The labels of the atomic positions are shown in Figure 1.

The O–O length varies from 1.570 Å for the Ca cluster (not shown in Table 2) versus 1.646 Å for the Zn one (Table 2), which is due to both the cationic size and the spatial restrictions being distorted relative to the experimental gas value $r_e = 1.201$ Å³⁵ or the theoretical value of 1.214 Å obtained at the B3LYP/6-31G* level. For comparison, the O···O distance varies from 2.560 Å in Al₂O₂³⁰ to 2.734 Å in Ga₂O₂.³¹ In order to evaluate the influence of the deformation of the MOR 8R ring on the Zn₂O₂ geometry, we performed a full geometry optimization without fixed H atoms which resulted in a highly symmetric 8R ring and rhomb Zn₂O₂ (Figure 1c). Table 2 shows that the geometrical parameters of the fully optimized rhomb Zn₂O₂ do not deviate essentially versus the optimization with spatially imposed restraints (Figure 1b), with the exception of the deviation from the plain rhomb Zn₂O₂ (Figure 1c) with a Zn14–O36–O35–Zn34 torsion angle of 161.86°. It signifies that the reactivity of the Zn₂O₂ cluster is not the result of a particular deformation in the 8R ring of MOR. We should add here that we did not succeed in optimizing the geometry of an isolated Zn₂O₂ cluster, i.e., without 8R fragment, neither at the B3LYP level, nor HF.

The ozone like O₃ part of the Me₂O₃ clusters has a similar angular (O—O—O) moiety of A-letter shape for both Me = Zn (Figure 1d) and Ca (Figure 1g), but the orientations of the O₃ are different relative to the cations (Table 4). The O—O distances and O—O—O angle of the O₃ part vary slightly between Zn₂O₃ (1.422 Å, 1.494 Å, 102.84°) and Ca₂O₃ (1.493 Å, 1.495 Å, 105.56°) at the B3LYP/6-31G* level. For Zn₂O₃, the two “legs”

TABLE 2: Several Geometrical Parameters of the Zn₂O₂(8R) Models (Distances in Å, Angles in Degrees) Calculated at the B3LYP/6-31G* Level with Full (−6542.707473 au) and Restrained (−6542.646315 au) Optimizations^a

parameter	full	restrained
Zn34—O35	1.920	1.912
Zn34—O36	1.920	1.895
Zn34...Al4	2.830	2.725
Zn14—O35	1.920	1.935
Zn14—O36	1.920	1.921
Zn14...Al17	2.830	2.859
O35—O36	1.648	1.646
Zn14...Zn34	3.468	3.417
Zn14—O35—Zn34	129.17	125.28
Zn14—O36—Zn34	129.17	127.07
O35—Zn34—O36	50.83	51.24
O35—Zn14—O36	50.83	50.55
Zn14—O36—O35—Zn34	179.96	161.86

^a The labels of the atomic positions are shown in Figure 2.

of the A-shape are linked to one of the two Zn cations whereas one of the two O atoms (O35) is also linked to the second Zn atom (Figure 1d). The same A-shape O₃ part for Ca₂O₃ is turned perpendicularly to the Ca···Ca axis and symmetrically coordinated to both Ca cations (Figure 1g). Two additional “inverted” and “rotated” isomers with local minimum for Ca₂O₃ were observed (Figure 1h,i) being less stable than the symmetric form (Figure 1g). The O₃ moiety keeps its O–O bonds and O–O–O angle in the “inverted” form (less stable by 26.6 kcal/mol at the B3LYP/6-31G* level, both Ca atoms are symmetrically oriented toward two O atoms of one O–O side of the O₃ part, Figure 1i) and the “rotated” form (less stable by 9.7 kcal/mol, Figure 1h). The rotated Ca₂O₃ conformer with the O–O distances of 1.497 and 1.504 Å and O–O–O angle of 105.34° corresponds to an approximate rotation by 90° of the symmetric form (Figure 1g) around the Ca···Ca axis. Different initial models were tested and led to the same conformers. The invariance of the O–O distances and O–O–O angle of the O₃ geometry confirms the stability of the Ca₂O₃ cluster. Additionally, we verified that the Zn type geometry as

TABLE 3: Mulliken Charges q (e) and Several Geometrical Parameters for the Me14-O35-Me34 Moiety of the $\text{Me}_2\text{O}(8\text{R})$ Models (Distances in Å, Angles in Degrees) Calculated at the B3LYP Level with Three Basis Sets for Me = Ca and with 6-31G* for Me = Zn^a

parameter	basis set (Me)			
	Ca/LANL1DZ	Ca/LANL2DZ	Ca/6-31G*	Zn/6-31G*
$q(\text{Me}14)$	1.342	1.170	0.913 ^b	0.776 ^d
$q(\text{O}35)$	-1.279	-1.115	-0.898 ^c	-0.811 ^e
Me14...Al17	3.131	3.247	3.247	2.945
Me14–O35	2.024	2.134	2.115	1.783
Me34–O35	2.021	2.136	2.118	1.766
Me14–O35–Me34	132.19	127.32	124.48	132.47

^a The 6-31G* basis is applied to the framework atoms. The labels of the atomic positions are shown in Figure 1. ^b NBO charge 1.792 e. ^c NBO charge -1.648 e. ^d NBO charge 1.608 e. ^e NBO charge -1.468 e.

TABLE 4: Several Geometrical Parameters of the $\text{Me}_2\text{O}_3(8\text{R})$ Models (Distances in Å, Angles in Degrees) Calculated at the B3LYP/6-31G* Level for Framework Atoms and 6-31G*(Me) or LANL2DZ(Me) Basis Set for the Me Cations, Me = Ca or Zn^a

parameter	Ca		Zn	
	LANL2DZ	6-31G*	LANL2DZ	6-31G*
Me34–O36	2.324	2.312	1.940	1.882
Me34–O35	2.532	2.513	2.080	2.066
Me34...O37	2.334	2.324	2.539	2.512
Me14...O36	2.347	2.336	3.848	3.854
Me14–O35	2.509	2.484	1.907	1.848
Me14...O37	2.336	2.328	2.728	2.696
O36–O37	1.493	1.493	1.422	1.422
O37–O35	1.498	1.495	1.499	1.494
Me14...Me34	3.686	3.661	3.709	3.709
O36–O37–O35	104.86	105.56	104.25	102.84

^a The labels of the atomic positions are shown in Figure 1d.

TABLE 5: Heats of Reactions (kcal/mol) of the Oxidation Reactions (eq 2, First Three Lines) and Heat of Reaction/Activation Barrier of CO Oxidation Reaction (eq 3a, Fourth Line) over the Me-Clusters (Me = Zn or Ca) Calculated at the B3LYP/6-31G* Level^a

reaction	Zn/6-31G*	Ca/6-31G*	Ca/LANL2DZ
$\text{Me}-\text{O}-\text{Me} + 1/2\text{O}_2 \rightarrow \text{Me}-\text{O}_2-\text{Me}$	-23.9	-24.8, -27.9 ^b	-35.7
$\text{Me}-\text{O}_2-\text{Me} + 1/2\text{O}_2 \rightarrow \text{Me}-\text{O}_3-\text{Me}$	39.0	-6.1, -12.7 ^b	-4.9
$\text{Me}-\text{O}-\text{Me} + \text{O}_2 \rightarrow \text{Me}-\text{O}_3-\text{Me}$	13.1	-30.9, -40.6 ^b	-40.6
$\text{Me}-\text{O}_2-\text{Me} + \text{CO} \rightarrow \text{Me}_2\text{CO}_3^c$	110.0/23.0, 114.3/18.8 ^{d,e} , 111.9/22.2 ^d , 104.2/24.1 ^f , 114.1/24.0 ^g , -/21.9 ^h	106.9/35.7, 108.6/33.5 ^d	108.1/31.5

^a 8R notation of the zeolite part with the Al-(O-Si)₃-O-Al alternation is omitted below for shortness. ^b At the MP2/6-31G* level. ^c Heat of reaction/activation barrier. ^d With extended cluster (+16 oxygen atoms, Figure 4). ^e LANL2DZ(Zn)/6-31G*(Si, Al, O, H, C) basis set. ^f At the B3PW91 level. ^g At the B3P86 level. ^h 6-311++G** basis set.

starting point for the Ca_2O_3 cluster led to the optimized symmetric form (Figure 1g). We here wish to add that all the details of geometry were equally well described for the Zn and Ca cations with the LANL2DZ basis versus the 6-31G* one (Table 4 for Ca_2O_3). The application of the LANL2DZ basis set will be much more important in future studies for heavier alkaline earth cations like Sr and Ba for which no 6-31G* basis set has been developed so far.

Finally, there is a qualitative difference between Zn and Ca versus the oxidation step from Me_2O_2 to Me_2O_3 . It is observed for the calculated heats of reaction of the possible catalytic cycle based on the series of consequent Me_2O_X oxide clusters (Table 5). All of the oxidation steps



by molecular oxygen from Me_2O to Me_2O_2 , from Me_2O_2 to Me_2O_3 , and from Me_2O_2 to Me_2O_3 are exothermic for Ca but not for Zn. For the latter, reaction (eq 2) is exothermic only for $X = 1$.

CO Oxidation over $\text{Me}_2\text{O}_2(8\text{R})$ Clusters. The presence of the O_2 moiety in Ca_2O_2 suggests the possible oxidation activity of the respective cation exchanged forms. Moreover, the consequent reaction steps (eq 2) for $X = 1$ and 2 together with CO oxidation to CO_2



could be the part of the closed catalytic cycle with participation of molecular O_2 . To check the catalytic activity, we considered CO oxidation to CO_2 (eq 3) which remains an important process from the industrial application and scientific points of view. The structures of the reagents (Figure 2a, d) are different for Zn (Figure 2a–c) and Ca (Figure 2d–f), whereas the structures of the transition states (TS) (Figure 2b, e) or products of CO oxidation (Figure 2c, f) are rather similar.

The $\text{CO}/\text{Zn}_2\text{O}_2(8\text{R})$ reaction complex (Figure 2a) differs from the geometry of the isolated $\text{Zn}_2\text{O}_2(8\text{R})$ cluster (Figure 1b) which is closer to the one of the TS complex (Figure 2b). The principal difference between the reaction and TS complexes is the shortening in the TS of the new C–O bond in the forming CO_2

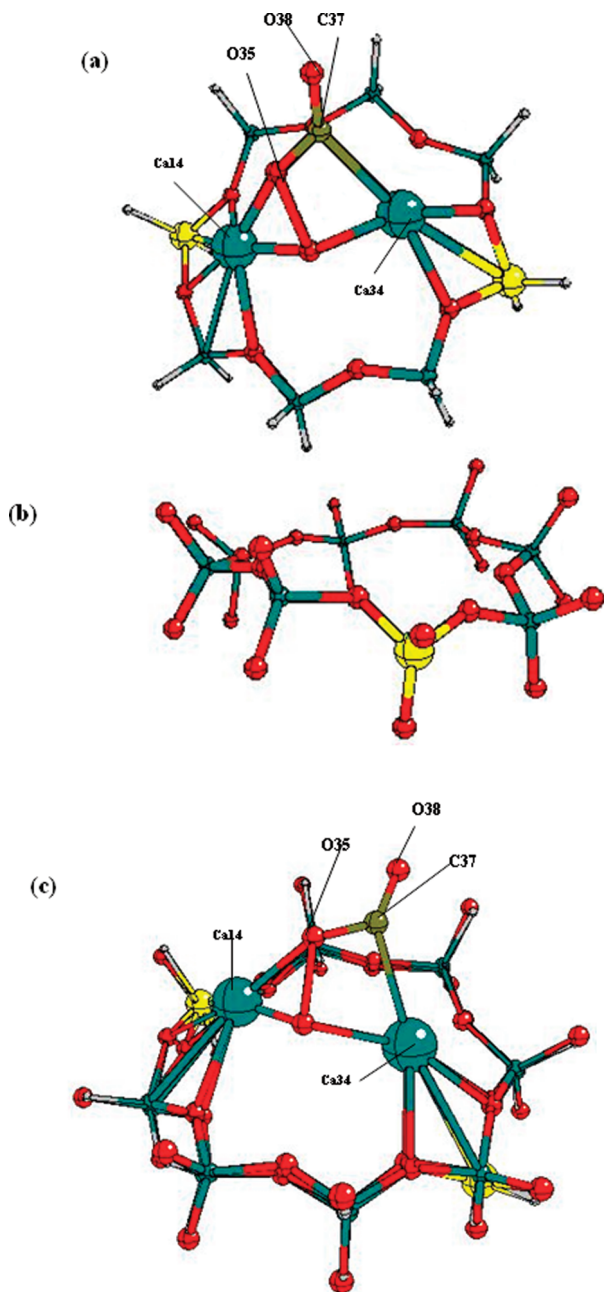


Figure 3. Structure of the optimized small cluster for the transition state of CO oxidation over $\text{Ca}_2\text{O}_2(8\text{R})$ (a), initial 8R ring of ZnMOR (b), and superimposed structures (c). The color code corresponds to the one of Figure 2.

molecule, i.e., 1.428 Å in the reaction complex and 1.284 Å in the TS, while the initial C–O one varies very little, i.e., 1.197 Å in the reaction complex versus 1.219 Å in the TS. The strong CO chemisorption over $\text{Me}_2\text{O}_2(8\text{R})$ results in a very high heat of adsorption of 18.7 and 13.3 kcal/mol for Me = Zn and Ca, respectively. We should add that the latter is nevertheless overestimated by at least 50% relative to the experimental heats of CO adsorption over the NaA,³⁶ i.e., 9.1 kcal/mol,³⁶ 6.1 kcal/mol over the NaA,³⁶ and 6.4–6.2 kcal/mol over the HMFI³⁷ zeolites.

On the opposite to the Zn cluster, $\text{Ca}_2\text{O}_2(8\text{R})$ holds its geometry in the reaction complex (Figure 2d). The Ca–C and Ca–O distances in the TS complex are much larger, i.e., 2.629, 2.852, and 2.405 Å for Ca34–C37, Ca34–O36, Ca14–O35 (using notations of Figure 2a) versus 2.093, 2.015, and 1.792 Å for the Zn–C and Zn–O distances in the TS of CO/

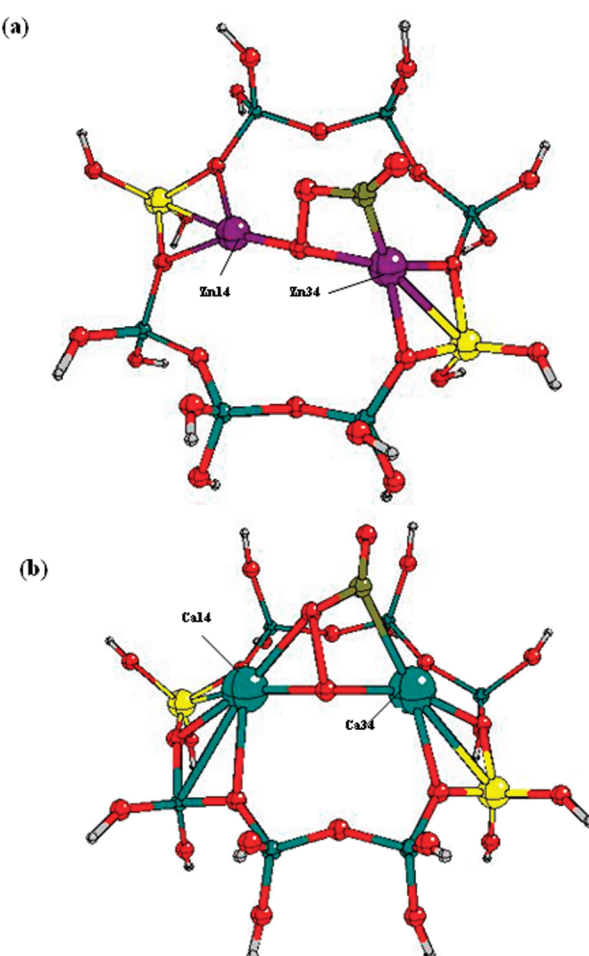


Figure 4. Structures of the extended optimized cluster for the transition state complexes for CO oxidation over $\text{Me}_2\text{O}_2(8\text{R})$ for Me = Zn (a) and Me = Ca (b). The color code corresponds to the one of Figure 2.

$\text{Zn}_2\text{O}_2(8\text{R})$ than the difference of 0.26 Å between the ionic radius of Zn and Ca.³² The minimal difference of 0.38 Å is between the Ca14–O36 and Zn14–O36 bonds, i.e., 2.216 versus 1.836 Å (Figure 2c).

The most stable products correspond to the CO_3^{2-} anion which is symmetrically coordinated to both Me cations for the Zn (Figure 2c) and Ca (Figure 2f) clusters



A closed catalytic cycle with participation of molecular O_2 can thus be realized provided that CO_2 could be desorbed from the $\text{Zn}_2\text{CO}_3(8\text{R})$ (Figure 2c) or $\text{Ca}_2\text{CO}_3(8\text{R})$ (Figure 2f) complex or from the less stable physisorbed CO_2 state for Zn form, for example by heating. The $\text{Zn}_2\text{CO}_3(8\text{R})$ product (Figure 2c) is more stable by 32.6 kcal/mol as compared to the physisorbed CO_2 molecule coordinated to only one Zn atom of $\text{Zn}_2\text{O}(8\text{R})$. Here, we should however add that the precise energy difference should be discussed while regarding accurately to the long-range effects for CO_2 adsorption. For the Ca case, CO_2 coordinates without energy barrier to both Ca cations of $\text{Ca}_2\text{O}_2(8\text{R})$, leading to $\text{Ca}_2\text{CO}_3(8\text{R})$ (Figure 2f). The indirect evidence of CO_3^{2-} formation is coming from spectroscopic data for CO/CaY at room as well as elevated temperatures.¹⁰ The time to remove CO_2 from CaY¹⁰ is longer as compared to the short time of CO removal, i.e., 3–4 min, which can be assigned to the appearance of the $\text{Me}_2\text{CO}_3(n\text{R})$ complex ($n = 4, 6$, or 12) in CaY. The

TABLE 6: Relative Stabilities ΔQ of the $\text{Ca}_2\text{O}_2(8R)$ Clusters, Respective Activation Barriers $\Delta E^\#$ of CO Oxidation, Heats of Reactions ΔU , and Imaginary Frequencies ω along the Reaction Coordinates Calculated at the B3LYP/6-31G* Level for Different $\text{Al}-(\text{O}-\text{Si})_n-\text{O}-\text{Al}$ Alternations Relative to the One for $n = 3^a$

n	ΔQ	$\Delta E^\#$	ΔU	$i\omega$
1	26.5	35.3	121.6	-673.7
2	15.8	37.7	121.7	-695.0
3	0.0	35.7	106.9	-750.3

^a All energy values are in kcal/mol, and frequencies are in cm^{-1} .

TABLE 7: $\Delta E^\#$ Activation Barriers of the $\text{Ca}_2\text{O}_3(8R) + \text{CO} \rightarrow \text{Ca}_2\text{CO}_4(8R)$ Oxidation Reaction, ΔE_{CO} Heat of CO Adsorption, ΔU Heat of Oxidation Reaction, and ΔE_{CO_2} Heat of CO_2 Adsorption, on Small $\text{Ca}_2\text{O}_3(8R)$ Cluster of MOR Calculated at the MP2 and B3LYP Levels Using the 6-31G* Basis Set for All Framework Atoms^a

energy values	B3LYP	MP2
$\Delta E^\#$	32.4	
ΔE_{CO}	12.4	15.1
ΔU	72.3	68.9
ΔE_{CO_2}	20.4	25.7

^a All values are in kcal/mol.

superimposed structures (Figure 3c) which were used to construct the extended cluster (Figure 4) allow to evaluate the distortion of the initial ring (Figure 3b) in course of the optimization (Figure 3a). Computations with the extended models (Figure 4) neither shift effectively the activation barrier, i.e., 33.5 and 22.2 kcal/mol instead of 35.7 and 23.0 kcal/mol for Ca- and Zn-clusters, respectively (Table 5), nor change the geometry of the systems. More details on the respective variations between the small and extended models are planned to be presented elsewhere.³⁸

Activation barriers were also evaluated using two other density functionals, B3PW91 and B3P86, that led to similar barrier values and TS geometries for $\text{CO}/\text{Zn}_2\text{O}_2(8R)$ (Table 5). To determine the reaction coordinate, we applied the QST3 algorithm as supplied with GAUSSIAN03.²⁸ Calculated imaginary frequencies along the respective reaction coordinates were $750.3i$, $877.5i$, and $878.2i \text{ cm}^{-1}$ for B3LYP, B3PW91, and B3P86, respectively. In all cases, the reaction coordinate corresponded to the vibrations of CO and one O atom of the Me_2O_2 group. For searching the geometries for the reaction complex, the TS, and the products, we also used the ONIOM approach of B3LYP/6-31G*:HF/3-21G type which converged for the reaction complex only, but not for TS and product complexes. The ONIOM result for the reaction complex nearly coincides with the geometry data obtained at the B3LYP/6-31G* level. The ONIOM models of the B3LYP/6-31G*:AM1 (or PM3 and UFF) type did not converge for the larger clusters.

Finally, geometry optimizations for the reagents and TS were performed at the B3LYP/6-311++G** level starting from the geometries obtained using B3LYP/6-31G*. It resulted in lower activation energy of 21.9 kcal/mol for the small $\text{CO}/\text{Zn}_2\text{O}_2(8R)$ cluster (Table 5). The variations of the heat of CO oxidation over the $\text{Me}_2\text{O}_2(8R)$ cluster do not exceed 5–6% relative to the value obtained at the B3LYP/6-31G* level, i.e., 110.0 kcal/mol for $\text{Me} = \text{Zn}$ and 106.9 kcal/mol for $\text{Me} = \text{Ca}$, when varying either the basis set, or the DFT functional (Table 5).

Tentatively, we also considered variations of the Al positions in the 8R ring for $\text{CO}/\text{Ca}_2\text{O}_2(8R)$, i.e., $\text{Al}-\text{O}-\text{Si}-\text{O}-\text{Si}-\text{O}-\text{Al}$ and $\text{Al}-\text{O}-\text{Si}-\text{O}-\text{Al}$; it did not result in principle differences

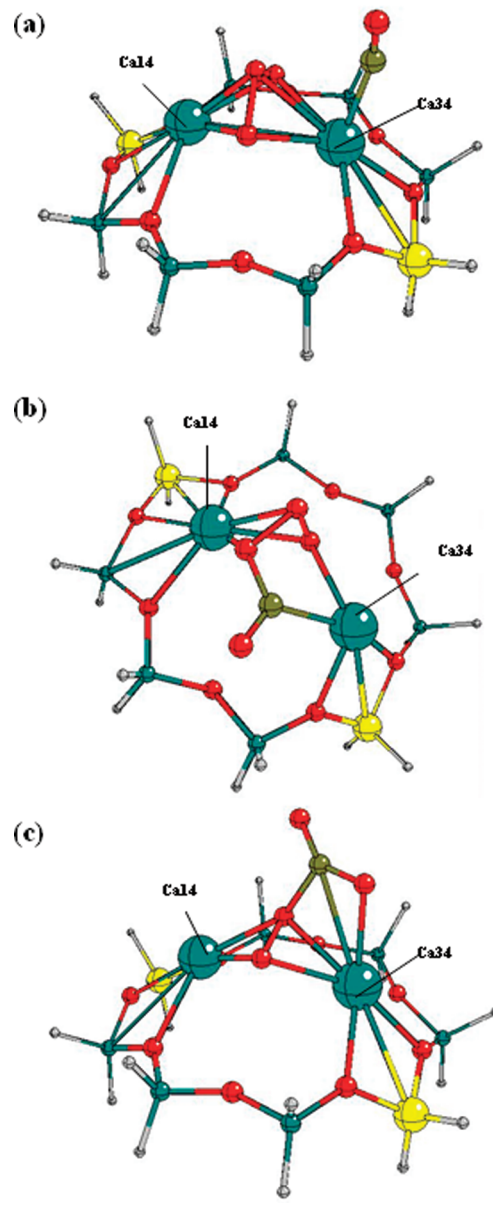


Figure 5. Structures of the reagent (a), transition state (b), and product clusters (c) for CO oxidation over the small optimized $\text{Ca}_2\text{O}_3(8R)$ cluster. The color code corresponds to the one of Figure 2.

regarding the activation energy values (Table 6). The respective reaction complexes are less stable by 15.8 and 26.5 kcal/mol than the $\text{Al}-\text{O}-\text{Si}-\text{O}-\text{Si}-\text{O}-\text{Al}$ type complex leading to activation barriers of 37.7 and 35.3 kcal/mol.

CO Oxidation over the $\text{Ca}_2\text{O}_3(8R)$ Cluster. We also checked the possibility of the $\text{Ca}_2\text{O}_3(8R)$ cluster for CO oxidation using the same type of process (eq 3a). This case turns out to be instructive regarding the evaluation of the reaction parameters at both the MP2 and B3LYP levels using the same 6-31G* basis set (Table 7). As CO is extremely sensitive to electron correlation effects, such a test is strongly required.

If both O atoms (Figure 2d) are nearly equivalent for $\text{Ca}_2\text{O}_2(8R)$, we tried to show which O atom could react first in the course of CO oxidation for $\text{Ca}_2\text{O}_3(8R)$. We found that any of the two extreme O atoms of the O_3 group can be involved in the CO_2 formation at the $\text{Ca}_2\text{O}_3(8R)$ cluster. The slightly lower activation energy for CO oxidation relative to the one is observed over $\text{Ca}_2\text{O}_2(8R)$, for example, 32.4 instead of 35.7 kcal/mol at the B3LYP/6-31G* level. The transition state (TS)

geometry turns out to be very similar to the case of CO oxidation over $\text{Ca}_2\text{O}_2(8R)$. The search of TS for CO over $\text{Ca}_2\text{O}_2(8R)$ at the MP2/6-31G* level is still in progress. The main differences between $\text{Ca}_2\text{O}_2(8R)$ and $\text{Ca}_2\text{O}_3(8R)$ in the course of oxidation are related to the heat of reaction which is much larger for $\text{Ca}_2\text{O}_2(8R)$, i.e., 106.9 (Table 6) versus 72.3 (Table 7) kcal/mol at the B3LYP/6-31G* level. We assigned this increase to the strong bidentate CO_2 chemisorption over $\text{Ca}_2\text{O}(8R)$ resulting in the CO_3^{2-} anion (Figure 2f). The more rigid geometry of the $\text{Ca}_2\text{O}_2(8R)$ product does not allow the same symmetric CO_3^{2-} coordination toward Ca_2O_2 (Figure 5).

On the basis of the data in Table 7, we conclude that electron correlation effects do not change qualitatively the reaction parameters at different computational levels but should however been checked from a quantitative point of view.

Conclusions

The oxidation activity of the Ca zeolite forms is well-known from literature. The oxidation mechanism for all cation exchanged zeolites is usually interpreted via “organic molecule– O_2 ” ion pair over a cation with an essential charge transfer. Nevertheless, it is difficult to apply such idea about ion pair stabilization for example to the $\text{CO}-\text{O}_2$ to explain CO oxidation occurring in Ca type zeolites. In this paper, another oxidation mechanism is suggested and discussed with respect to CO oxidation for Zn- and Ca-cation exchanged zeolites.

Different geometries of Me_2O_2 and Me_2O_3 oxide moieties in fragments of the 8R ring of mordenite (MOR) were first modeled for Me = Zn and Ca at the B3LYP/6-31G* level via the cluster approach. For Zn, the Zn_2O_2 and Zn_2O_3 moieties are oriented in a plane that is nearly perpendicular to the 8R ring and passes through both Zn cations. The Zn_2O_2 geometry is very similar to the square type clusters already calculated for Al_2O_2 and Ga_2O_2 , and partly confirmed experimentally for Ga_2O_2 ; however, the O–O bond is much shorter in Zn_2O_2 . The rhomb type Ca_2O_2 moiety is parallel to the 8R ring due to the spatial restrictions for the larger Ca cation so that both O atoms are available for adsorbate molecules as compared to the Zn_2O_2 one. The O_3 type fragment in $\text{Me}_2\text{O}_3(8R)$ conserves the common A-letter shape which is oriented notably asymmetrically in the Zn_2O_3 cluster and symmetrically in the Ca_2O_3 cluster, this last one being elevated over the 8R ring and cations. The heats of $\text{Ca}_2\text{O}_X(8R)$ oxidation by molecular oxygen calculated at the B3LYP/6-31G* level were confirmed at the MP2/6-31G* level for $X = 1$ and 2, both being of the same order of value.

We observed a difference between the possible catalytic cycles based on a series of consequent Ca_2O_X or Zn_2O_X oxides. All of the oxidation steps by molecular oxygen from Ca_2O to Ca_2O_2 , from Ca_2O to Ca_2O_3 , and from Ca_2O_2 to Ca_2O_3 are exothermic, whereas for Me = Zn only one step from Zn_2O to Zn_2O_2 is exothermic. However, a lower activation barrier for oxidation according to the $\text{Me}_2\text{O}_2(8R) + \text{CO} \rightarrow \text{Me}_2\text{CO}_3(8R)$ reaction was obtained for Me = Zn versus Me = Ca. A more complete relaxation of the whole moiety including CO oxidation at Me_2O_2 was further considered by adding a layer of 16 oxygen atoms connected to all Si and Al atoms. All computations with the extended models or using other DFT correlation functionals, PW91, P86, neither shifted effectively the activation barrier, nor changed the geometry for the Me = Zn systems.

Essentially lower heats of CO oxidation according to the $\text{Ca}_2\text{O}_X(8R) + \text{CO} \rightarrow \text{Ca}_2\text{CO}_{X+1}(8R)$ reaction was obtained for $X = 3$ versus $X = 2$. It was explained due to non complete chemisorption of CO_3^{2-} obtained near the more rigid $\text{Ca}_2\text{O}_2(8R)$ fragment. The heat of CO oxidation over $\text{Ca}_2\text{O}_3(8R)$ computed

at the B3LYP/6-31G* level was confirmed at the MP2/6-31G* level as well as the heats of CO and CO_2 adsorption. The closeness between the heats of adsorption calculated at the DFT and MP2 levels proves the accuracy of the B3LYP evaluations regarding the thermodynamic parameters for the CO oxidation processes. Respective activation energies were found to be close for $X = 2$ and 3 for the reaction above at the B3LYP/6-31G* level.

Hence, we could suggest the possible realization of closed oxidation catalytic cycle based on the series of the Ca_2O_X and Zn_2O_X oxide clusters at the cationic positions of the zeolites with moderate value of Si/Al modulus.

Acknowledgment. The authors thank the FUNDP, the FNRS-FRFC, and the Loterie Nationale (Convention 2.4578.02) for the use of the Namur Interuniversity Scientific Computing Facility (iSCF) Centre. The authors also acknowledge the CGRI for financial support in the framework of the Programme de la coopération 2008–2010 entre la Communauté française de Belgique, la Région wallonne et la Fédération de Russie (convention 2008/18342).

References and Notes

- (1) Blatter, F.; Frei, H. *J. Am. Chem. Soc.* **1993**, *115*, 7501.
- (2) Blatter, F.; Moreau, F.; Frei, H. *J. Phys. Chem.* **1994**, *98*, 13403.
- (3) Blatter, F.; Frei, H. *J. Am. Chem. Soc.* **1994**, *116*, 1812.
- (4) Sun, H.; Blatter, F.; Frei, H. *J. Am. Chem. Soc.* **1994**, *116*, 7951.
- (5) Sun, H.; Blatter, F.; Frei, H. *J. Am. Chem. Soc.* **1996**, *118*, 6873.
- (6) Panov, A. G.; Larsen, R. G.; Totah, N. I.; Larsen, S. C.; Grassian, V. H. *J. Phys. Chem. B* **2000**, *104*, 5706.
- (7) Larsen, R. G.; Saladino, A. C.; Hunt, T. A.; Mann, J. E.; Xu, M.; Grassian, V. H.; Larsen, S. C. *J. Catal.* **2001**, *204*, 440.
- (8) Xu, J.; Mojet, B. L.; van Ommen, J. G.; Lefferts, L. *J. Phys. Chem. B* **2005**, *109*, 18361.
- (9) Visser, T.; Nijhuis, T. A.; van der Eerden, A. M. J.; Jenken, K.; Ji, Y. Y.; Bras, W.; Nikitenko, S.; Ikeda, Y.; Lepage, M.; Weckhuysen, B. M. *J. Phys. Chem. B* **2005**, *109*, 3822.
- (10) Shete, B. S.; Kamble, V. S.; Gupta, N. M.; Kartha, V. B. *J. Phys. Chem. B* **1998**, *102*, 5581.
- (11) Delgass, W. N.; Garten, R. L.; Boudart, M. *J. Phys. Chem.* **1969**, *73*, 2970.
- (12) Garten, R. L.; Delgass, W. N.; Boudart, M. *J. Catal.* **1970**, *18*, 90.
- (13) Dalla Betta, R. A.; Garten, R. L.; Boudart, M. *J. Catal.* **1976**, *41*, 40.
- (14) Chen, H.-Y.; El-Malki, El.-M.; Wang, X.; van Santen, R. A.; Sachtler, W. M. H. *Catalysis by unique metal ion structures in solid matrices*; NATO science series II; Genti, G., Ed.; Kluwer Acad. Publ.: Dordrecht, The Netherlands, 2001; Vol. 13, pp 75–84.
- (15) Lei, G. D.; Adelman, B. J.; Sarkany, J.; Sachtler, W. M. H. *Appl. Catal., B* **1995**, *5*, 245.
- (16) El-Malki, El.-M.; van Santen, R. A.; Sachtler, W. M. H. *J. Catal.* **2000**, *196*, 212.
- (17) Sayle, D. C.; Catlow, C. R. A.; Gale, J. D.; Perrin, M. A.; Nortier, P. *J. Phys. Chem. A* **1997**, *101*, 3331.
- (18) Teraishi, K.; Ishida, M.; Irisawa, J.; Kume, M.; Takahashi, Y.; Nakano, T.; Nakamura, H.; Miyamoto, A. *J. Phys. Chem. B* **1997**, *101*, 8079.
- (19) Catlow, C. R. A.; Bell, R. G.; Gale, J. D.; Lewis, D. W.; Sayle, D. C.; Sinclair, P. E. *Catalytic activation and functionalization of light alkanes*; Derouane, E. G., Ed.; Kluwer: Dordrecht, The Netherlands, 1998; pp 189–214.
- (20) Goodman, B. R.; Schneider, W. F.; Hass, K. C.; Adams, J. B. *Catal. Lett.* **1998**, *56*, 183.
- (21) Yakovlev, A. L.; Shubin, A. A.; Zhidomirov, G. M.; van Santen, R. A. *Cat. Lett.* **2000**, *70*, 175.
- (22) Yakovlev, A. L.; Zhidomirov, G. M.; van Santen, R. A. *J. Phys. Chem. B* **2001**, *105*, 12297.
- (23) Hansen, N.; Heyden, A.; Bell, A. T.; Keil, F. J. *J. Phys. Chem. C* **2007**, *111*, 2092.
- (24) Gale, J. D. *GULP 1.3*; Royal Institution/Imperial College: UK, 1992/1994.
- (25) Schröder, K. P.; Sauer, J.; Leslie, M.; Catlow, C. R. A.; Thomas, J. M. *Chem. Phys. Lett.* **1992**, *188*, 320.
- (26) Gale, J. D.; Henson, N. J. *J. Chem. Soc. Faraday Trans.* **1994**, *90*, 3175.

- (27) Yuan, S.; Wang, J.; Li, Y.; Peng, S. *J. Mol. Catal. A* **2001**, *175*, 131.
- (28) *Gaussian 03*, Revision C.02; Frisch, M. J., Gaussian, Inc., Wallingford, CT, 2004.
- (29) Barbosa, L. A. M. M.; van Santen, R. A. *J. Phys. Chem. C* **2007**, *111*, 8337.
- (30) Zhidomirov, G. M.; Larin, A. V.; Trubnikov, D. N.; Vercauteren, D. P. in preparation.
- (31) Zhidomirov, G. M.; Shubin, A. A.; Milov, M. A.; Kazansky, V. B.; van Santen, R. A.; Hensen, E. J. M. *J. Phys. Chem. C* **2008**, *112*, 3321.
- (32) Hensen, E. J. M.; Pidko, E. A.; Rane, N.; van Santen, R. A. *Angew. Chem., Int. Ed.* **2007**, *46*, 7273.
- (33) Shannon, R. D. *Acta Cryst. A* **1976**, *32*, 751.
- (34) Lacheen, H. S.; Iglesia, E. *Chem. Mater.* **2007**, *19*, 1877.
- (35) Huber, K. P.; Herzberg, G. *Molecular Spectra and Molecular Structure; Constants of Diatomic Molecules*; Van Nostrand: New York, 1976; Vol. 4.
- (36) Masuda, T.; Tsutsumi, K.; Takahashi, H. *J. Colloid Interface Sci.* **1980**, *77*, 238.
- (37) Savitz, S.; Myers, A. L.; Gorte, R. J. *J. Phys. Chem. B* **1999**, *103*, 3687.
- (38) Zhidomirov, G. M.; Larin, A. V.; Trubnikov, D. N.; Vercauteren, D. P. *J. Mol. Struct.* submitted for publication.

JP808449W